

Electrically tunable g-factors in quantum dot molecular spin states

M. F. Doty^{1,*}, M. Scheibner¹, I. V. Ponomarev¹, E. A. Stinaff¹, A.

S. Bracker¹, V. L. Korenev², T. L. Reinecke¹, and D. Gammon¹

¹Naval Research Laboratory, Washington, DC 20375, USA and

²A.F. Ioffe Physical Technical Institute, St. Petersburg 194021, Russia

(Dated: July 6, 2021)

We present a magneto-photoluminescence study of individual vertically stacked InAs/GaAs quantum dot pairs separated by thin tunnel barriers. As an applied electric field tunes the relative energies of the two dots, we observe a strong resonant increase or decrease in the g-factors of different spin states that have molecular wavefunctions distributed over both quantum dots. We propose a phenomenological model for the change in g-factor based on resonant changes in the amplitude of the wavefunction in the barrier due to the formation of bonding and antibonding orbitals.

PACS numbers: 75.40.Gb, 78.20.Ls, 78.47.+p, 78.67.Hc

Quantum Dots and Quantum Dot Molecules (QDMs) have proven to be a versatile medium for isolating and manipulating spins [1, 2], which are of great interest for quantum information processing [3, 4]. In particular, photoluminescence (PL) spectra have been used in self-assembled QDMs to observe coherent tunneling [5, 6, 7, 8] and identify spin interactions through fine structure [9]. Electrical control of isolated spins through their g-factors is highly desirable for implementation of quantum gate operations. To date, electrical control of g-factors has only been observed in ensembles of electrons in quantum wells by shifting the electron wavefunctions into different materials [10, 11, 12, 13]. In this Letter we present a striking electric field resonance in the g-factor for molecular spin states confined to a single quantum dot molecule.

To our knowledge this is the first observation of electrical control over the g-factor for a single confined spin. Moreover, the isolation of a single QDM allows us to spectrally resolve and identify individual molecular spin states that have different g-factor behaviors. In Fig. 1a we indicate molecular spin states of both the neutral exciton (X^0 , one electron recombining with one hole) and positive trion (X^+ , electron-hole recombination in the presence of an extra hole) at zero magnetic field. The different electric field dependences of the g-factors for these states is apparent in Fig. 1b, where the splitting of PL lines increases for some molecular spin states and decreases for others. This electric field dependence is nearly an order of magnitude larger than previously reported in quantum wells [10, 11, 12, 13]. The effect arises from the formation of bonding and antibonding orbitals, which results in a change in the amplitude of the wavefunction in the barrier at resonance.

Our QDMs consist of two vertically stacked self-assembled InAs dots truncated at a thickness of 2.5 nm and separated by a 2 nm GaAs tunneling barrier [14]. As an applied electric field tunes the relative energies of the two dots, strong tunnel coupling between the hole states creates the molecular spin states. Unlike samples

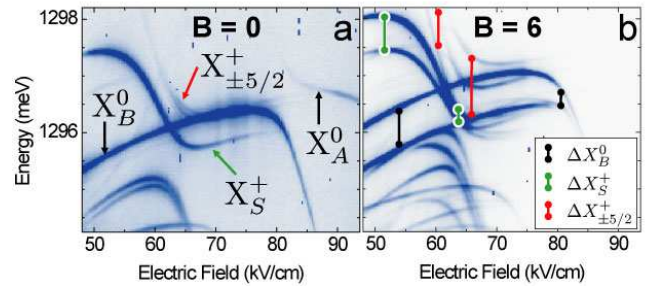


FIG. 1: (a) $B = 0$ T photoluminescence spectra of a single QDM. The complex pattern of anticrossings arises from the formation of molecular spin states. (b) At $B = 6$ T, the molecular spin states have a Zeeman splitting (bars) that depends strongly on the applied electric field (F).

with a thicker tunnel barrier [5], the states retain molecular character throughout the observed range of electric fields. We present data from a single molecule, but the universality of the behavior has been verified by detailed studies of 7 other molecules from the same sample. We first explain the spectra and molecular spin states at $B = 0$ T. We then describe the magnetic field dependence and propose a phenomenological model for the electric field dependent Zeeman splitting.

In Fig. 2 we show all PL lines from X^0 and X^+ at $B = 0$ T. These lines are identified by their relative energies, the power dependence of their intensities and the electric field dependence of the anticrossings [5]. The X^0 lines (Fig. 2a) show a clear anticrossing at F_{X^0} . The anticrossing arises from tunnel coupling between the ground state hole levels in each dot, which forms bonding (X_B^0) and antibonding (X_A^0) orbitals. The electron remains in the bottom dot throughout the range of electric fields considered here [5]. The X^+ lines (Fig. 2b) have a more complicated pattern because anticrossings occur in both the initial (one electron and two holes) and final (one hole) states [5, 9].

To explain the origin of the X^+ molecular spin states

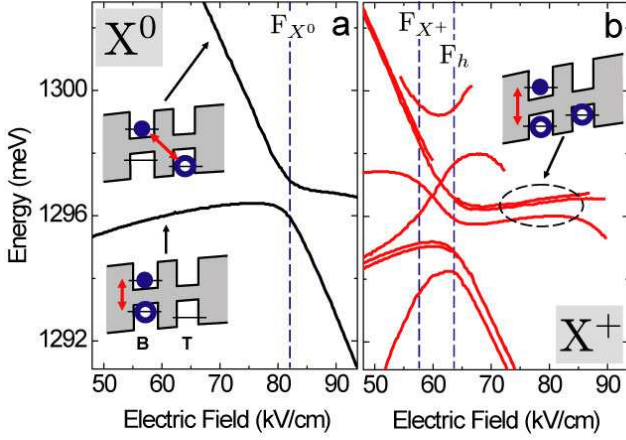


FIG. 2: Energies extracted from Fig. 1a. (a) X^0 lines anticross at F_{X^0} , where the direct (lower inset) and indirect (upper inset) transitions are degenerate. (b) X^+ initial states anticross at F_{X^+} and near 90 kV/cm. Final (hole) states anticross at F_h . Inset: charge distribution for the circled singlet and triplet transitions.

we turn to the Hamiltonians. The basis states will be identified as ${}^{e_B, e_T}_{h_B, h_T} X_k^Q$, where e_B [e_T] are the spins of electrons ($\pm 1/2$: \uparrow or \downarrow) and h_B [h_T] the spins of heavy holes ($\pm 3/2$: \uparrow or \downarrow) in the bottom [top] dot. X indicates an exciton (h a single hole) and Q is the net charge. k is the total spin projection. Singlets, which have total spin $\pm 1/2$, will be denoted X_S to distinguish them from the $\pm 1/2$ triplets.

The final state has only a single hole with relative energies given by the diagonalization of the Hamiltonian:

$$\hat{H}^h = \begin{pmatrix} 0 & t_h \\ t_h & e\tilde{d}F \end{pmatrix} \quad (1)$$

in the spin degenerate ${}^{0,0}_{\uparrow,0} h^+_{+3/2}$, ${}^{0,0}_{0,\uparrow} h^+_{+3/2}$ basis, where t_h is the tunneling energy for a bare hole, \tilde{d} is the distance between dot centers and F is the applied electric field. The energies of the final states as a function of electric field are shown in Fig. 3b. The formation of bonding and antibonding states at the anticrossing point is illustrated.

The initial state (X^+) contains one electron and two holes. For simplicity we present only the electron-spin-up case, which is degenerate with the spin-down case at zero magnetic field. If both holes are in the same dot, the Pauli principle requires singlet configurations: ${}^{\uparrow,0}_{\uparrow\downarrow,0} X^+_S$ (both in the bottom dot) or ${}^{\uparrow,0}_{0,\uparrow\downarrow} X^+_S$ (both in the top dot). If there is one hole in each dot, singlet (${}^{\uparrow,0}_{\downarrow,\uparrow} X^+_S$) and triplet (${}^{\uparrow,0}_{\downarrow,\uparrow} X^+_{+1/2}$, ${}^{\uparrow,0}_{\downarrow,\downarrow} X^+_{-5/2}$, ${}^{\uparrow,0}_{\uparrow,\uparrow} X^+_{+7/2}$) configurations are possible. By ${}^{\uparrow,0}_{\downarrow,\uparrow} X^+_S$ we mean the antisymmetric hole spin wavefunction ($\downarrow, \uparrow - \uparrow, \downarrow$). ${}^{\uparrow,0}_{\downarrow,\uparrow} X^+_{+1/2}$ means the symmetric hole spin wavefunction ($\downarrow, \uparrow + \uparrow, \downarrow$). The relative

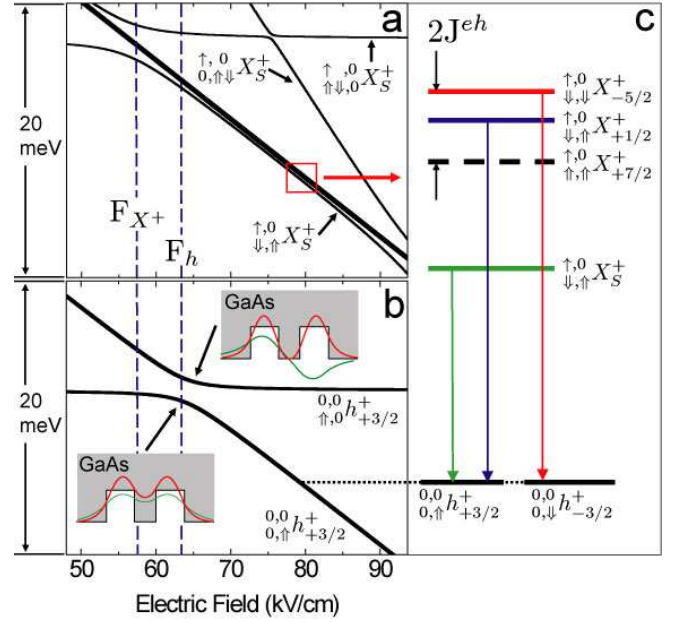


FIG. 3: Calculated zero magnetic field energies of spin-degenerate (a) initial states (X^+) and (b) final states (h^+) [15]. Labels indicate the dominant basis state for easy comparison to Eq. 2. Insets in (b) show the bonding (lower) and antibonding (upper) wavefunctions (green) and probability distributions (red). (c) Fine structure of singlet and triplet states at $F = 79.2$ kV/cm. Arrows indicate optically allowed transitions to the bonding final state.

energies of the initial states are given by the Hamiltonian:

$$\hat{H}^{X^+} = \begin{pmatrix} \Gamma_1 & t_{X^+} & 0 & 0 & 0 & 0 \\ t_{X^+} & e\tilde{d}F & J^{eh} & 0 & 0 & t_{X^+} \\ 0 & J^{eh} & E_{+1/2} & 0 & 0 & 0 \\ 0 & 0 & 0 & E_{-5/2} & 0 & 0 \\ 0 & 0 & 0 & 0 & E_{+7/2} & 0 \\ 0 & t_{X^+} & 0 & 0 & 0 & 2e\tilde{d}F + \Gamma_2 \end{pmatrix} \quad (2)$$

in the ${}^{\uparrow,0}_{\uparrow\downarrow,0} X^+_S$, ${}^{\uparrow,0}_{\downarrow,\uparrow} X^+_S$, ${}^{\uparrow,0}_{\downarrow,\uparrow} X^+_{+1/2}$, ${}^{\uparrow,0}_{\downarrow,\downarrow} X^+_{-5/2}$, ${}^{\uparrow,0}_{\uparrow,\uparrow} X^+_{+7/2}$, ${}^{\uparrow,0}_{0,\uparrow\downarrow} X^+_S$ basis. Γ_1 and Γ_2 are due to Coulomb interactions, t_{X^+} is the Coulomb-corrected tunneling energy for a hole in the presence of an electron and additional hole, $E_k = e\tilde{d}F + mJ^{eh}$ with $m = 0, +1, -1$ for $k = +1/2, -5/2, +7/2$. J^{eh} is the exchange energy between an electron and hole in the same dot [5, 16]. Diagonalizing Eq. 2 gives the energies of the initial states, which are plotted as functions of electric field in Fig. 3a.

Because tunneling is a spin conserving process, only the ${}^{\uparrow,0}_{\downarrow,\uparrow} X^+_S$ singlet state can tunnel couple with ${}^{\uparrow,0}_{\uparrow\downarrow,0} X^+_S$ and ${}^{\uparrow,0}_{0,\uparrow\downarrow} X^+_S$, which must be singlets because the two holes are in the same dot. These 3 singlets are therefore strongly mixed to create molecular orbital states that anticross near 57 kV/cm (F_{X^+}) and 90 kV/cm. Unlike the

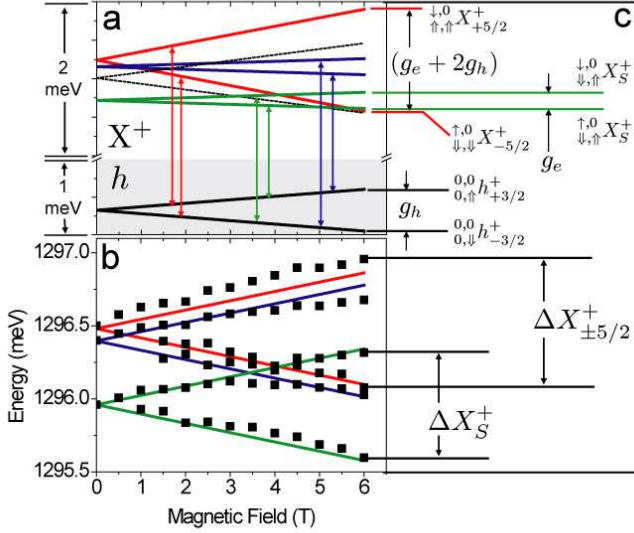


FIG. 4: (a) Magnetic field dependence of initial (\$X^+\$) and final (\$h\$) states for the singlet and triplet transitions at an electric field of 79.2 kV/cm (schematic Fig. 3c). Vertical lines indicate spin allowed recombinations. (b) Calculated (colored lines) and experimentally observed (black points) PL energies. (c) Zeeman splitting of PL lines (\$\Delta\$) and initial and final states for \$X^+_{\pm 5/2}\$ (red lines) and \$X^+_{\pm 5/2}\$ (green lines).

singlet states, the triplet states do not mix and are not affected by these anticrossings [17]. This creates a “kinetic” splitting between triplet and singlet states [18]. An example is indicated by the dashed oval in Fig. 2b, where the lower energy singlet line remains separated from the two optically allowed triplet lines, which are split by electron-hole exchange. The fine structure of the corresponding states is shown in Fig. 3c.

By adding the Zeeman interaction to the Hamiltonian [19], we calculate the magnetic field dependence of the molecular spin states. Fig. 4a shows the states of Fig. 3c, which split into doublets with an applied longitudinal magnetic field. The final states are simply the two spin orientations of a single hole, split by \$g_h\$. The splitting of initial states depends on their spin configuration. Due to the two parallel hole spins, \$X^+_{\pm 5/2}\$ has a large splitting given by \$g_e + 2g_h\$ while \$X^+_{\pm 7/2}\$ is split by \$-g_e + 2g_h\$. In contrast, the \$\pm 1/2\$ singlet (\$X^+_S\$) and triplet (\$X^+_{\pm 1/2}\$) have oppositely paired hole spins and therefore a small splitting given by \$g_e\$. The g-factor for PL transitions is given by the difference in g-factor between the initial and final states. Away from the electric field resonances, the g-factor is \$g_T = g_e + g_h\$, as indicated by the vertical lines.

Using the model described below, we obtain \$g_T = -2.2\$. To plot the initial and final states in Fig. 4a we have taken the relative weights of the electron and hole g-factors to match those obtained by Bayer: \$g_e = -0.6\$ and \$g_h = -1.6\$ [19]. The calculated energies of the transitions are shown by the lines in Fig. 4b. The experi-

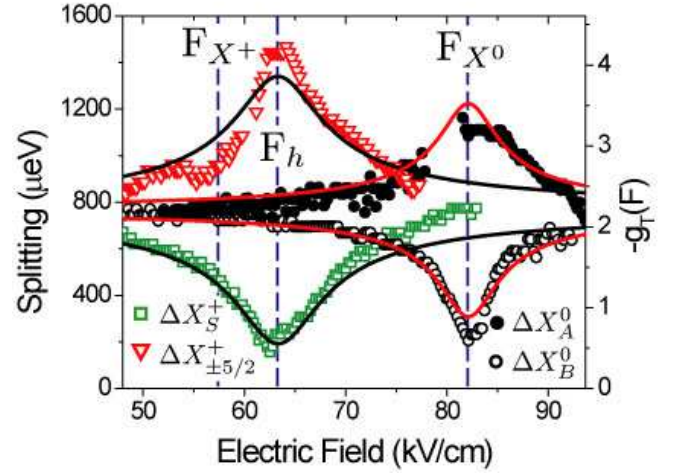


FIG. 5: Zeeman splitting and corresponding g-factor, \$g_T\$, as a function of electric field at \$B = 6\$ T.

mentally observed PL energies are given by the symbols, with the diamagnetic shift (\$10.9 \mu\$eV/T\$^2\$) subtracted.

The g-factor resonances are clearly evident in Fig. 5, where the symbols plot the measured energy splitting of the \$X^0\$ and two \$X^+\$ Zeeman doublets at \$B = 6\$ T as a function of electric field. Strong enhancement or suppression of the splitting is observed at \$F_h\$ and \$F_{X^0}\$. All of the data can be qualitatively explained by a phenomenological model of the formation of bonding and antibonding orbitals, which results in resonant changes in the amplitude of the wavefunction in the barrier. We focus first on transitions involving a bonding orbital (open symbols), which have an increased amplitude of the wavefunction in the barrier (Fig. 3b lower inset).

The wavefunction for the bonding orbital of a single hole can be written as \$\Psi_B = a|1\rangle + b|2\rangle\$, where \$|1\rangle\$ and \$|2\rangle\$ are the basis states of Eq. 1, the wavefunctions for holes localized in the two different dots. The coefficients \$a\$ and \$b\$ are functions of electric field determined by Eq. 1. The electric field-dependent g-factor for a hole in a bonding orbital is given by \$g_h^B(F) = \langle \Psi_B | g_h(z) | \Psi_B \rangle\$, where \$g_h(z)\$ is the hole g-factor as a function of position in the sample. \$g_h(z)\$ is taken as a phenomenological parameter, in part because the degree of alloying between the nominally pure InAs dots and GaAs barrier is unknown [20].

If we assume that the g-factors for the holes localized in each dot are the same, we get \$g_h^B(F) = g_h + 2abg_{12}\$, where \$g_{12} = \langle 1 | g_h(z) | 2 \rangle\$ gives the contribution from the amplitude of the wavefunction in the barrier. In the case of the \$X^+_S\$ singlet (shown in Figs. 3c and 4c), the initial states are split by \$g_e\$, so the total transition g-factor is given by

$$g_T^B(F) = g_e + g_h^B(F) = g_T + \frac{2t_h g_{12}}{\sqrt{e^2 \tilde{d}^2 (F - F_h)^2 + 4t_h^2}} \quad (3)$$

where the explicit form for $2ab$ determines the lineshape centered around the anticrossing point F_h .

The lower black line in Fig. 5 is obtained by fitting Eq. 3 to ΔX_S^+ . Using the measured values of t_h (0.86 meV) and F_h (63.3 kV/cm) we find $g_{12} = 1.65$. The barrier contribution is positive, like the heavy hole g-factor in bulk GaAs (~ 1.05) [21, 22]. Because g_T and g_{12} have opposite sign, the splitting reaches a minimum at F_h , where the amplitude in the barrier is at a maximum. The g-factor at the minimum is -0.44 .

Because the $\pm 5/2$ triplet states recombine to the same bonding orbital of the final hole (Fig. 3), the model predicts the splitting of these lines as a function of electric field with no additional fitting. As shown in Fig. 4c, the $\pm 5/2$ triplet states have an initial state splitting of $g_e + 2g_h$. The transition g-factor is therefore given by $g_T^B(F) = (g_e + 2g_h) - (g_h + 2abg_{12}) = g_T - 2abg_{12}$. This is shown by the upper black line, which matches $\Delta X_{\pm 5/2}^+$, the observed splitting of the $\pm 5/2$ triplets. The maximum splitting corresponds to a g-factor of -4.23 .

To apply the g-factor model to the bonding orbital of the neutral exciton (lower branch Fig. 2a) we use the measured tunneling energy ($t_{X^0} = 0.58$ meV) and anticrossing field ($F_{X^0} = 82.1$ kV/cm). The lower red line in Fig. 5 shows the fit to ΔX_B^0 , the Zeeman splitting of PL lines from the bonding orbital. We find $g'_{12} = 1.32$. The electron-hole Coulomb interaction is responsible for the difference in tunneling energy and anticrossing field from the bare hole case and is also likely responsible for the difference between g_{12} and g'_{12} . The g-factor at the minimum is -0.59 .

Using this value of g'_{12} , the model immediately explains the increase in splitting for the antibonding orbital (upper branch Fig. 2a), which has a *reduced* wavefunction amplitude within the barrier. The g-factor for the antibonding orbital is given by $g_T^A(F) = g_T - 2abg'_{12}$, which *increases* in magnitude at the resonant field because g_T is negative and g'_{12} is positive. This is shown by the upper red line in Fig. 5, which matches ΔX_A^0 , the Zeeman splitting for excitonic recombination from the antibonding orbital. The splitting increases to a maximum (g-factor -3.35) at the anticrossing point. The antibonding transitions for X^+ show similar behavior, but are too weak to obtain full resonance curves.

The overall agreement between the model and experimental data is quite good. There are some minor discrepancies, which highlight the need for a detailed theory, possibly requiring inclusion of excited states [23]. However, the agreement of the data with the resonance linewidths calculated using independently measured values of t_{X^0} and t_h is strong confirmation that the g-factor dependence does arise from the formation of bonding and antibonding orbitals. For X^+ the g-factor resonance arises from the wavefunction of the single hole in the final state, while for X^0 the orbital wavefunction of the hole is influenced by the additional electron.

We also studied samples in which electrons tunnel through the barrier, with an anticrossing energy (~ 2.3 meV) comparable to that of the hole tunneling sample presented here (~ 1.7 meV). This requires a thicker barrier (10 nm) because of the smaller electron effective mass. The electron wavefunction amplitudes in the barrier should be at least as large as the hole-tunneling case. However, the electron g-factor in bulk GaAs (-0.44) [24] is similar to the electron g-factor in InAs quantum dots (-0.6) and according to our model the contribution from the barrier should not significantly change the electron g-factor. We see no electric field dependence of the g-factor in these electron anticrossing samples. By adding aluminum to the barrier, the resonant contribution to the electron g-factor could be enhanced.

We have presented a resonant change in g-factor as a function of electric field for the molecular spin states of QDMs with a thin tunnel barrier. By studying single QDMs, we are able to identify the individual molecular spin states and the different resonant behavior of their g-factors. The results suggest that design of molecular spin states and tunnel resonances may provide new opportunities for combining optical and electrical control of confined spins.

We acknowledge financial support by NSA/ARO, CRDF, RFBR, RSSF, and ONR. E.A.S., I.V.P., and M.F.D. are NRC/NRL Research Associates.

* Electronic address: doty@bloch.nrl.navy.mil

- [1] F. H. L. Koppens, *et al.*, Science **309**, 1346 (2005).
- [2] J. R. Petta, *et al.*, Science **309**, 2180 (2005).
- [3] D. Loss and D. P. DiVincenzo, Phys. Rev. A **57**, 120 (1998).
- [4] R. Vrijen, *et al.*, Phys. Rev. A **62**, 012306 (2000).
- [5] E. A. Stinaff, *et al.*, Science **311**, 636 (2006).
- [6] H. J. Krenner, *et al.*, Phys. Rev. Lett. **94**, 057402 (2005).
- [7] H. J. Krenner, *et al.*, cond-mat/0604659 (2006).
- [8] G. Ortner, *et al.*, Phys. Rev. Lett. **94**, 157401 (2005).
- [9] M. Scheibner, *et al.*, cond-mat/0607241 (2006).
- [10] G. Salis, *et al.*, Nature **414**, 619 (2001).
- [11] M. Poggio, *et al.*, Phys. Rev. B **70**, 121305(R) (2004).
- [12] H. W. Jiang and E. Yablonovitch, Phys. Rev. B **64**, 041307(R) (2001).
- [13] Y. Lin, *et al.*, Physica E **21**, 656 (2004).
- [14] Dots are MBE grown on GaAs [5] in a diode structure; an Al mask with 1 μ m apertures isolates single QDMs.
- [15] Numerical values from experimental spectra: $\Gamma_1 = 3.2$ meV, $\Gamma_2 = 13.1$ meV, $t_h = 0.86$ meV, $t_{X^+} = 1.24$ meV, $J^{eh} = 0.116$ meV, $\tilde{d} = 4.29$ nm.
- [16] We can not rule out a small direct exchange energy between holes in separate dots, J^{hh} . Because the anticrossing near 90 kV/cm is not fully observed, we can not separate J^{hh} from the kinetic singlet-triplet splitting due to tunneling. Since the kinetic splitting is dominant in these samples we have, for simplicity, taken $J^{hh} = 0$.
- [17] The $\uparrow_{\downarrow, \uparrow}^0 X_{\pm 1/2}^+$ states mix slightly with $\uparrow_{\downarrow, \uparrow}^0 X_S^+$ through

electron-hole exchange, J^{eh} [9].

- [18] P. Fazekas, *Lecture Notes on Electron Correlation and Magnetism* (World Scientific, Singapore, 1999).
- [19] M. Bayer, *et al.*, Phys. Rev. B **61**, 7273 (2000).
- [20] Our values of $g_e = -0.6$ and $g_h = -1.6$ are typical for InAs QDs. For bulk GaAs, $g_h \sim 1.05$ for heavy holes and $g_e = -0.44$ [21]. Zeeman splittings for both electrons and holes are given by $g\mu_B B$.
- [21] V. A. Karasyuk, *et al.*, Phys. Rev. B **49**, 16381 (1994).
- [22] M. J. Snelling, *et al.*, Phys. Rev. B **45**, 3922(R) (1992).
- [23] There is evidence that the first excited hole state is ~ 7 meV higher in energy. ($\Delta F \sim 16$ kV/cm).
- [24] H. Kosaka, *et al.*, Elect. Lett. **37**, 464 (2001).